Biochimica et Biophysica Acta 1858 (2016) 2498–2511

Contents lists available at ScienceDirect

Biochimica et Biophysica Acta

journal homepage: www.elsevier.com/locate/bbamem

An overview of molecular dynamics simulations of oxidized lipid systems, with a comparison of ELBA and MARTINI force fields for coarse grained lipid simulations☆

P. Siani [a,b], R.M. de Souza [b], L.G. Dias [b], R. Itri [c], H. Khandelia [a,*]

[a] MEMPHYS-Center for Biomembrane Physics, Department of Physics and Chemistry, University of Southern, Denmark
[b] Departamento de Química, FFCLRP, Universidade de São Paulo, Ribeirão Preto, SP, Brazil
[c] Departamento de Física Aplicada, Instituto de Física, Universidade de São Paulo, São Paulo, SP, Brazil

ARTICLE INFO

Article history:
Received 27 January 2016
Received in revised form 23 March 2016
Accepted 24 March 2016
Available online 6 April 2016

Keywords:
Oxidized phospholipids
Molecular dynamics
Coarse-grained
Free energy
Water permeation
Lipid mixing

ABSTRACT

Biological membranes and model lipid systems containing high amounts of unsaturated lipids and sterols are subject to chemical and/or photo-induced lipid oxidation, which leads to the creation of exotic oxidized lipid products (OxPLs). OxPLs are known to have significant physiological impact in cellular systems and also affect physical properties of both biological and model lipid bilayers. In this paper we (i) provide a perspective on the existing literature on simulations of lipid bilayer systems containing oxidized lipid species as well as the main related experimental results, (ii) describe our new data of all-atom and coarse-grained simulations of hydroperoxidized lipid monolayer and bilayer systems and (iii) provide a comparison of the MARTINI and ELBA coarse grained force fields for lipid bilayer systems. We show that the better electrostatic treatment of interactions in ELBA is able to resolve previous conflicts between experiments and simulations. This article is part of a Special Issue entitled: Biosimulations edited by Ilpo Vattulainen and Tomasz Róg.

1. Introduction

Lipids of biological membranes contain predominantly high amounts of monounsaturated and polyunsaturated acyl chains. Model lipid vesicles also often contain a significant proportion of unsaturated acyl tails. These are susceptible to lipid oxidation, which leads to the creation of exotic chemical species, some of which resemble lipids, but have hydrophilic group pendant on the sometimes shortened acyl oxidized lipid chains. Such oxidized lipid products (OxPLs) can remain in the membrane, and add to already complex composition of membranes and have a major impact on the physical properties of membranes as well as cell physiology (Catalá [12]). Quite remarkably, it has been shown that oxidized lipids can play important roles in diseases as Parkinson and Alzheimer [57,68,71] atherosclerosis [78,80] diabetes, aging and carcinogenesis induced by UV and in physiology processes (generation of defense response, signaling molecules and hormones) [21,24,58].

The chemical transformations that take place in the start of the lipid oxidation are well established, although the progression that the peroxidation occurs through intermediates is not yet well characterized. Poly-unsaturated lipids can start the oxidation reaction by themselves by easily losing an alyllic hydrogen and starting a radical chain reaction. Single unsaturated phospholipids and cholesterol need a highly oxidizing compound such as hydroxyl radical or singlet oxygen to start the oxidation process. Both light and chemically induced oxidation reactions usually start with the formation of a lipid hydroperoxide, which can be further oxidized [31]. There is considerable information supporting the hypothesis that lipid hydroperoxides not only start the oxidation chain reactions but also alter the properties of the membranes, by changing fluidity, packing thickness, lipid–lipid interaction and organization and raft structure and dynamics to initiate signaling pathways [31,74]. Moreover, the formation of oxidized lipids with shortened alkyl chains also changes the properties of the membranes, and may lead to the formation of pores [28,72] and membrane disruption [11]. In model lipid systems, lipid oxidation is likely to occur from shining of high intensity light to fluorescent probes and photosensitizer molecules used in microscopy experiments [4,26]. The formation of oxidized lipids is likely to alter the phase diagram of such model lipid mixtures that usually contain a low-melting point unsaturated lipid.

From the simulation point of view, there have been a host of simulation studies during the last decade (partially reviewed by Jurkiewicz et al. [34]) with different oxidized lipid species that describe the impact of OxPLs on model lipid bilayer systems. In the

☆ This article is part of a Special Issue entitled: Biosimulations edited by Ilpo Vattulainen and Tomasz Róg.

* Corresponding author.
E-mail address: hkhandel@sdu.dk (H. Khandelia).

http://dx.doi.org/10.1016/j.bbamem.2016.03.031
0005-2736/

current review we will provide our perspective of prior simulations of OxPL containing model systems. We will also describe our new simulations of hydroperoxidized lipids using all-atom force fields and the ELBA coarse grained force field [18,59–62], which are aimed at resolving some discrepancies between prior simulations and experiments of hydroperoxidized lipid bilayers. In this context, we also compare the performance of the ELBA and the popular MARTINI [2,16,30,49–51,55,64,66,84,85,87,91,92] force field, and show that the electrostatic treatment of interactions in ELBA is able to reproduce experimentally observed properties of bilayers containing oxidized lipid species. In Scheme 1, we summarize the structures of OxPLs discussed throughout the paper. We will not focus on oxysterols, antioxidants and reactive oxygen species in model membranes owing to lack of space. However, recent computer simulations have also addressed these issues. The reader can go to [15,19,20,42,43,63,81] for in-depth details.

2. Simulations of the oxidized phospholipids

2.1. All-atom simulations

2.1.1. Bilayers

In the first investigation of the impact of oxidized phospholipids on mimetic membranes using Molecular Dynamics (MD) Simulation (Wong-Ekkabut et al. [94]), the authors described the effect of lipid oxidation on 1-palmitoyl-2-linoleoyl-*sn*-glycero-3-phosphatidylcholine (PLPC) phospholipid bilayers. Aldehyde and hydroperoxide chemical groups were attached at the carbon 9 and carbon 13 positions totaling to four different oxidation products. Simulations were based on Berger force field [7] using the SPC water model [95]. The average bilayer area increased with increasing content of oxidized phospholipids (OxPLs) because of the tendency of the polar oxidized groups to reside at the water interface, thus bending the oxidized lipid tail. For instance,

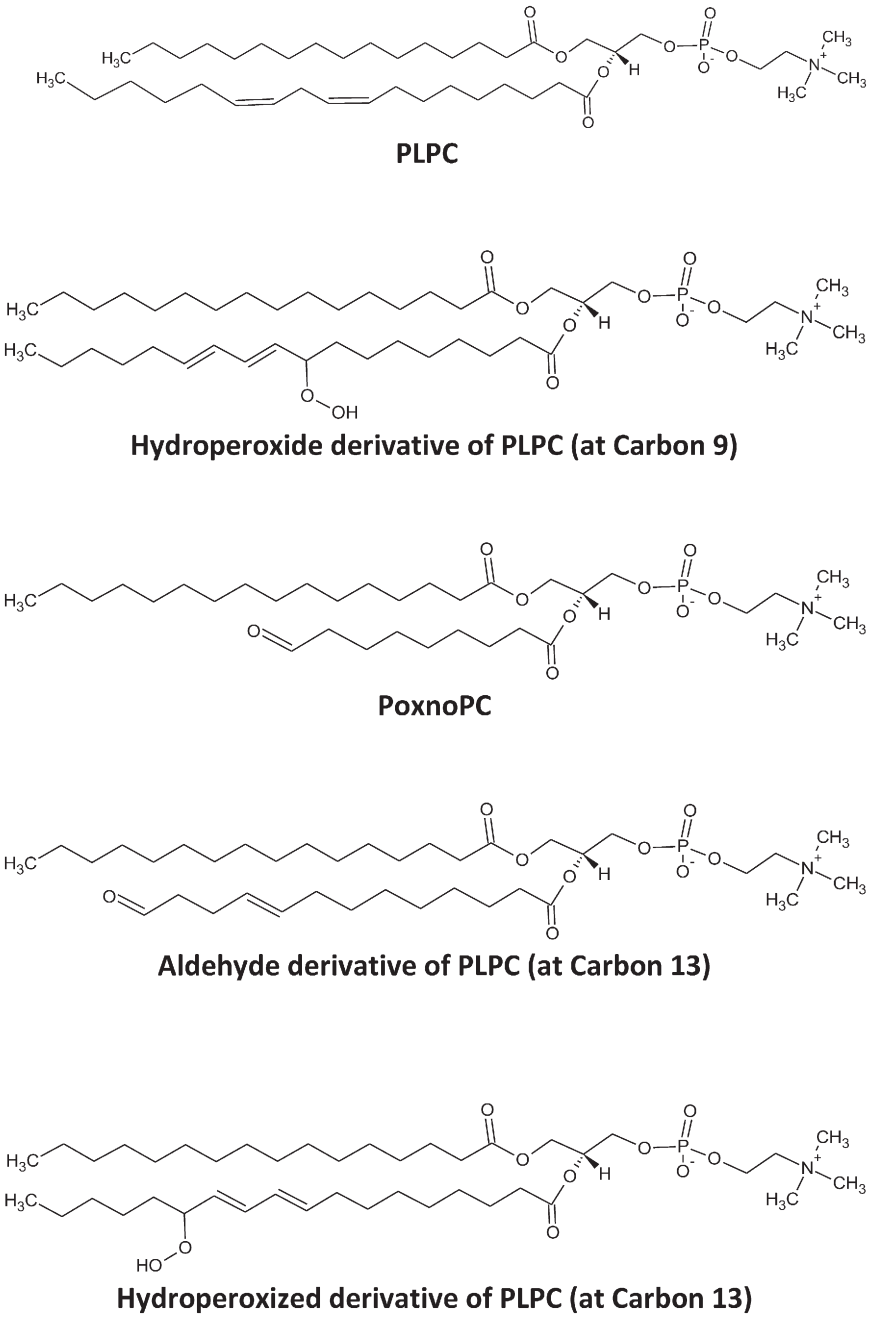

Scheme 1. Planar representation of the lipids present in the lipid mixtures that were simulated.

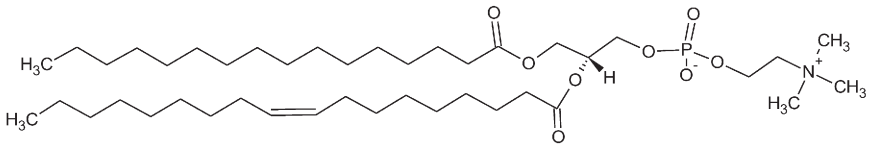

POPC

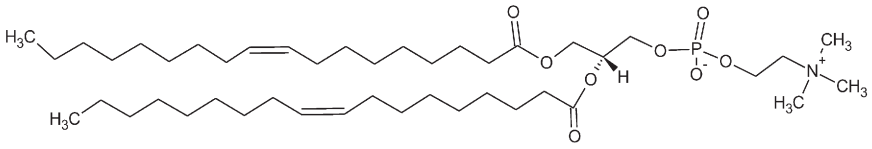

DOPC

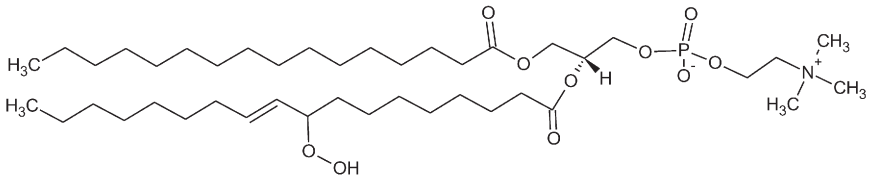

POPC-OOH

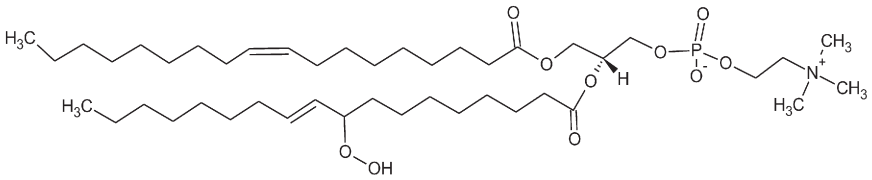

DOPC-OOH

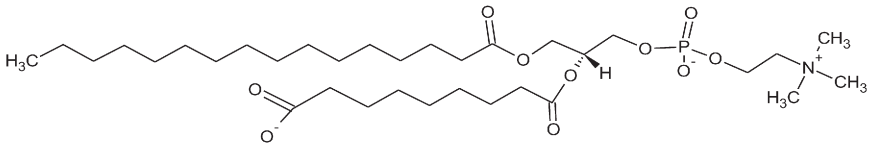

PazePC

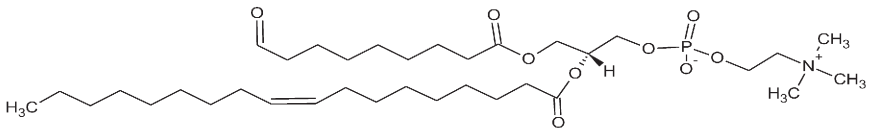

Ox1PC

Scheme 1 (*continued*).

with 50% of oxidized lipids, the area per lipid increased from 65 Å^2 to 69 Å^2 and 72 Å^2, in the case of hydroperoxide group linked to the C9 and C13 positions, respectively. Such an increase was also experimentally observed by *in situ* photo-oxidation of giant unilamellar vesicles (GUVs) composed of either 1-palmitoyl-2-oleoyl-*sn*-glycero-3-phosphocholine (POPC) or 1,2-dioleoyl-*sn*-glycero-3-phosphocholine (DOPC) containing a small amount of photosensitizer molecule [56,70,74,93]. Such an area increase results from the addition of a hydroperoxide group to the C9 (or C10) position of the unsaturated chain due to the photo-chemical reaction of singlet oxygen to the double bond of the acyl chain [31,74]. Such an increase in area will be further discussed later below.

The increase in area per lipid was accompanied by a decrease of the bilayer thickness determined by a shift of the polar head-group electron density peaks towards the bilayer core, leading to an increased density in the hydrocarbon region. A decrease in the order parameter in the oxidized *sn*-2 tails was also observed. The disordering effect was more pronounced in the *sn*-2 chains containing aldehyde groups than those containing hydroperoxides. DPH fluorescence anisotropy experimental results also suggest a decrease

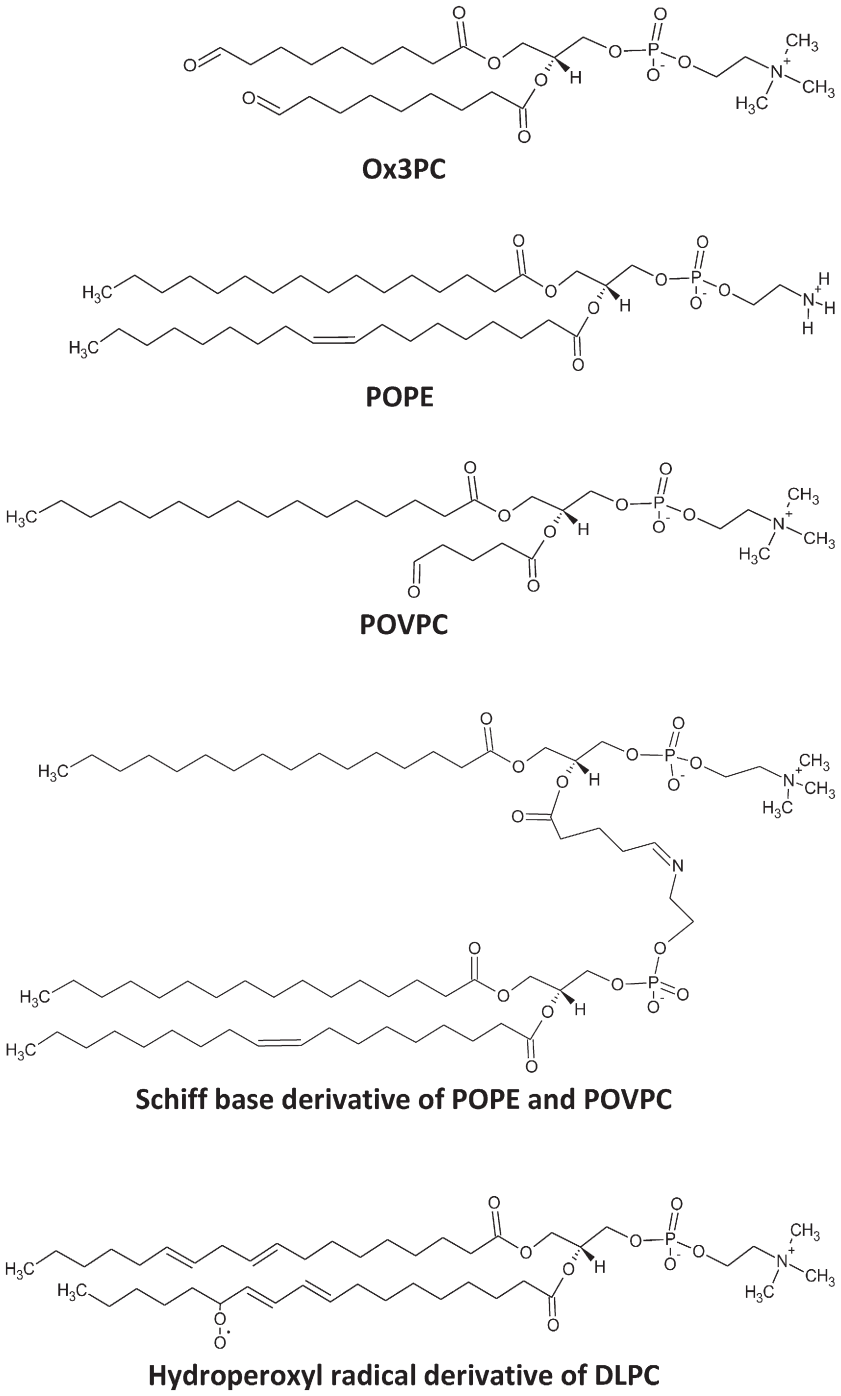

Scheme 1 (*continued*).

in the order parameter in phosphatidylcholine bilayers containing a certain percentage of similar OxPLs [34].

Water permeability through the bilayers with higher OxPLs concentrations also increased, suggesting a possible cell damage mechanism due to this phenomenon (Wong-Ekkabut et al. [94])). However, GUVs formed by hydroperoxized-POPC (POPC-OOH) or hydroperoxized-DOPC (DOPC-OOH) did not show any apparent change in water permeability during the controlled photo-oxidation process [93].

A remarkably enhanced lipid transbilayer diffusion and water penetration in the presence of oxidized lipids was demonstrated by Volinsky et al. [89]) using fluorescence and MD simulations. Notably, the free-energy barrier for flip-flop corresponding to the translocation of a single lipid molecule from water bulk to the bilayer core decreased by approximately 5 kcal/mol when 20% of oxidized lipids (PoxnoPC) were present in the POPC membrane.

A different class of OxPLs with shortened chains were simulated by Khandelia and Mouritsen [39]). They were: the 1-palmitoyl-2-(9′-oxo-nonanoyl)-*sn*-glycero-3-phosphocholine (PoxnoPC) and 1-Palmitoyl-2-azelaoyl-*sn*-glycero-3-phosphocholine (PazePC) lipids. Both the CHARMM [47] and the Berger force fields [7] were used. PoxnoPC and PazePC have aldehyde and carboxylate groups at the end of their truncated *sn*-2 chains, respectively. For both force fields, the truncated tails of PazePC completely reversed orientation, thus exposing its carboxyl group to aqueous phase, in very good agreement with Förster-type resonance energy transfer (FRET) results obtained between Cytochrome-c and fluorescently labeled PazePC model membranes [54].

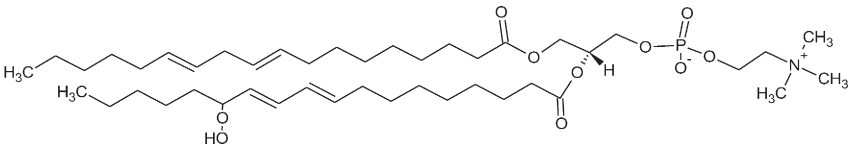

Hydroperoxized derivative of DLPC

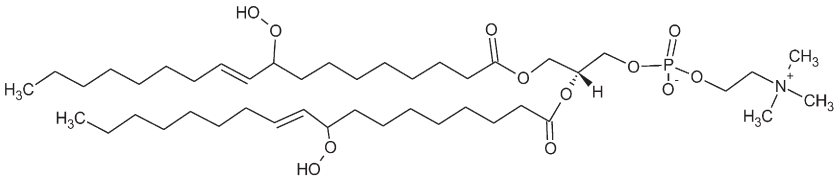

DOPC-2OOH

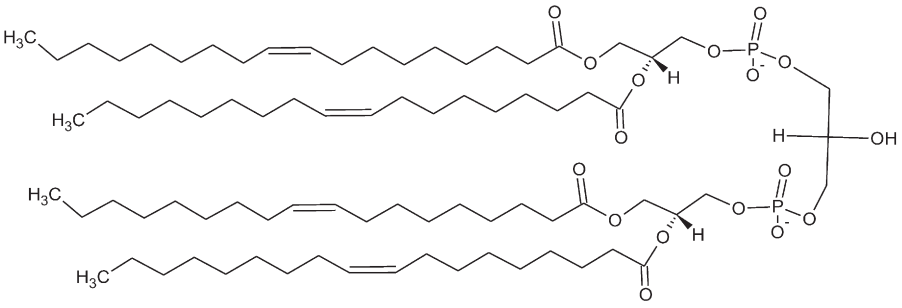

CLP

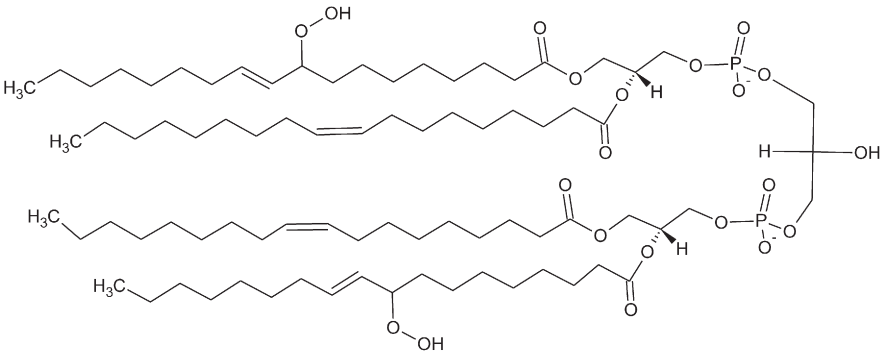

CLP-2OOH

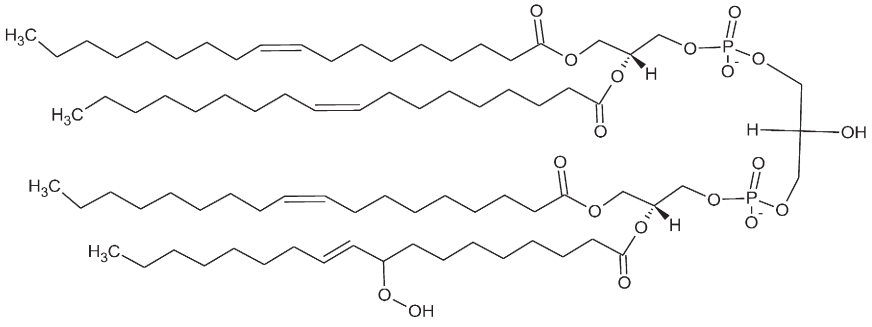

CLP-OOH

Scheme 1 (*continued*).

Interestingly, disruption of DOPC GUVs dispersed in methylene blue solution under irradiation was associated to the formation of shortened-chain DOPC lipids as a result of the photo-oxidation process [11]. More recently, Cwiklik and Jungwirth showed (Berger force-field for the lipids and SPC for water model) that high content of truncated chains with the aldehyde functional group promoted membrane disruption within a few nanoseconds (Cwiklik and Jungwirth 2010). However, in systems contain just one of the two unsaturated chains of DOPC oxidized to aldehyde, the integrity of the lipid bilayer was preserved. When the two unsaturated lipid tails were oxidized, micellization naturally followed because of the lack of any bilayer forming molecules in the system.

Such pore formation was also investigated in mixtures comprising different proportions of DOPC lipids, 1-(9′-oxo-nonanoyl)-2-oleoyl-sn-glycero-3-phosphocholine (OX1PC) and nonanal molecules [46] with oxidized species ranging from 15% to 90%, using the Berger force field [7] for lipids and the SPC model for water [95]. The OxPLs were generated by cleavage of DOPC lipids at the double bonds present in the sn-1 acyl chains and subsequent addition of an aldehyde group. Water clusters in the headgroup region were noticed for the lipid bilayers containing 15 to 66% of OxPLs, whereas pore formation followed by water penetration across the membrane was observed when lipid oxidation ratio was over 75%. Water permeation across the membrane was enhanced upon insertion of OxPLs compounds and remained constant after pore formation. The Berger force field for lipids and the SPC model for water were employed.

The effect of three specific POPC lipid peroxidation products and cholesterol on the properties of POPC phospholipid bilayer were studied by Van der Paal et al. [86]) using the united atom GROMOS 43A1-S3 force field [13] and parameters for the peroxide and aldehyde group obtained by Wong-Ekkabut et al. [94]). The simulated POPC peroxide compounds comprise the hydroperoxide and aldehyde functional form, inspired by the experimental characterization of the principal products of POPC lipid obtained under oxidative stress conditions by Reis et al. [69]) using reversed-phase liquid chromatography–mass spectrometry. A decrease in the lipid order upon oxidation and pore formation in the systems containing aldehyde compounds was noticed. For systems containing hydroperoxide compounds, or when cholesterol content exceeded 11%, pore formation was not observed. Due to the reduced presence of cholesterol in the plasma membrane of cancer cells [83] compared to healthy cells, the authors suggest that cancer cells are more vulnerable to the consequences of lipid peroxidation. Cholesterol's protective effect on oxidized lipid membranes was also observed by simulations [38,79]. Recent simulations (Boonnoy et al. [9])) also show that compared to hydroperoxide groups, OxPLs containing aldehyde-moieties make PLPC bilayers more susceptible to pore formation. Interestingly, photo-induced oxidative stress on GUVs composed of DOPC and cholesterol revealed that cholesterol protects the membrane from oxidative damage even though it is also prone to oxidation [35]. From the experimental point of view, the study of light-induced oxidation of POPC and DOPC GUVs reveals a two-stage process [56, 74]: initially GUVs present high-amplitude fluctuations due to increase in surface area as a result from hydroperoxide group formation adjacent to the chain double bond as described above. As oxidation continues, the GUVs return to their original rigid spherical shape, followed by increase in membrane permeability due to nano-scale pores [56] and/or micro-scale pores formation [56,74]. Increased vesicle rigidity and pore formation are ascribed to further chemical changes of the lipid molecules with tail scission into shortened acyl chain capped with alcohol and aldehyde groups as probed by NMR results [74]. Interestingly, it has been shown that the kinetics of pore formation is dependent on the lipid species [56], and is faster for DOPC than for POPC. Furthermore, the first oxidation step that generates hydroperoxide groups is one order of magnitude faster than the step which produces truncated acyl chains and pores [74].

Hermetter et al. [27] used the modified Berger force field [7] and SPC water model [95] to study an exotic class of OxPLs, which are formed from Schiff base condensation between a 1-palmitoyl-2-oleoyl-*sn*-glycero-3-phosphoethanolamine (POPE) lipid and 1-palmitoyl-2-(5′-oxo-valeroyl)-*sn*-glycero-3-phosphocholine (POVPC). The new OxPL, a phospholipid having three hydrocarbon tails and two head groups significantly increased the average cross-sectional area (area per lipid) and decreased the bilayer thickness.

Using the CHARMM36 force field [29,40] and the TIP3P water model [33], Garrec et al. [22] investigated the validity of the *floating peroxyl radical* hypothesis, and showed that the peroxyl radical did not *float* at the surface of the membrane. Hydroperoxized tails of OxPLs stay close to the headgroup region due to the preferential hydrogen bond interactions with the carbonyl groups. Similar behavior was also observed with the Berger force field (Wong-Ekkabut et al. [94]).

To summarize existing all-atom simulations of oxidized lipids: all simulations focusing on hydroperoxized molecules point to a decrease in the membrane bilayer thickness and order parameters accompanied by a concomitant increase in the lateral area. The preferred position of the electron density profile (EDP) maxima peaks for hydroperoxized groups is close to carbonyl groups, and hydroperoxide groups do not induce pore formation independent of the water model and force field employed.

The availability of experimental data of light-induced oxidation on GUVs formed by hydroperoxized-POPC and hydroperoxized-DOPC [56,70,74,93] and the absence of atomistic MD studies involving the DOPC phospholipid containing both chains hydroperoxized, led us to investigate the hydroperoxized DOPC and POPC using the CHARMM36 force field [40] and TIP3P water model [33], with parameters available from Garrec et al. [22]. The results obtained by atomistic simulations also were utilized as *reference* in the calibration process of new equivalent CG models (Section 2.2.2). Due to the presence of two unsaturated tails in the DOPC, two types of hydroperoxized DOPC were studied: one model containing only one hydroperoxized tail (named DOPC-OOH), and other containing two hydroperoxized tails (named DOPC-2OOH), both at the Carbon 9 position (the hydroperoxized POPC is named POPC-OOH) as shown in Scheme 1.

The electron density profiles for DOPC-OOH, DOPC-2OOH and POPC-OOH bilayers show that the hydroperoxide group resides close to the interface and that there is an increased water penetration into the bilayer (Fig. 1). Such a unimodal profile for the hydroperoxide group is in good agreement with previous work [22,94]. The preferred position for the hydroperoxide group was between 7 and 10 Å with respect to the bilayer center.

Unlike truncated oxidized lipid tails, hydroperoxized tails feel an *anchor effect*, generated by the methylene groups in the aliphatic tail after the hydroperoxide group, thus keeping it internalized. The effect is counter-balanced by a strong attraction of carbonyl group to the bilayer interface. This *anchor effect* is absent in truncated oxidized hydrocarbon tails, allowing greater mobility for these OxPLs.

Jarerattanachat et al. [32]) suggested that the ability of hydroperoxide groups to make hydrogen bonds with water molecules below the interfacial region is independent of the hydroperoxide concentration in the systems. Our data also shows that the maximum in the electron density profile for the hydroperoxide group remains unaltered with increasing hydroperoxide concentration.

The *sn*-2 tails containing hydroperoxide group have lower order parameters compared to the same *sn*-2 chains in pure non-OxPLs systems (Fig. 2). In both systems, there is larger disorder in the region, which precedes the hydroperoxide group, occurring between Carbon 2 and Carbon 8, wherein the movement of the bonds between C5 and C10 is random. The region below the hydroperoxide group (C10 onwards) is not affected significantly.

Additional information about the dynamics of the oxidized *sn*-2 lipid tails and the hydroperoxide group were obtained by analysis of the tilt angle distributions (Θ_N) with respect to the membrane plane normal, shown (Fig. 3). For the hydroperoxide group, a hydroperoxide vector coinciding with its dipole moment was used, and for the oxidized

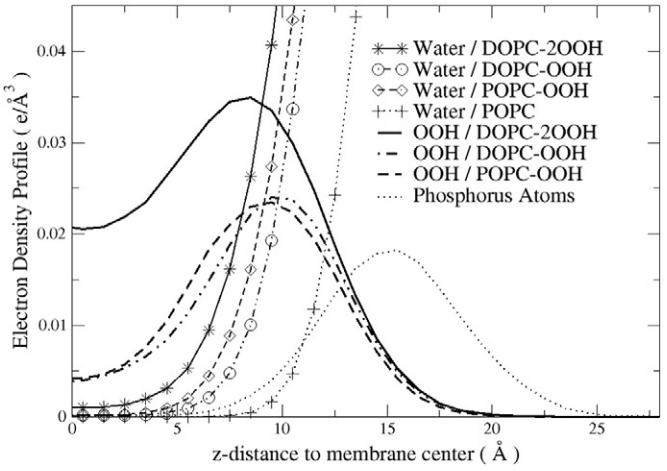

Fig. 1. Electron density profile (EDP) for water and the hydroperoxide group in the DOPC-OOH, DOPC-2OOH, POPC-OOH and POPC bilayers. The phosphorus atom EDP was plotted as a guide to visualize the approximate position of the bilayer-water interface.

chain a vector from the first to the last carbon was used to measure tilt angles. The peak for the average angle distributions for all *sn*-2 oxidized tails (Θ_{tail}) was ~140°, showing similar average tilt angles compared to nonoxidized POPC *sn*-2 chains about 160°–180° ([6]), as a direct result of *anchor effect* on hydroperoxidized tails. The angle distributions for polar hydroperoxide group (Θ_{OOH}) occurs at ~50°, driven by polar interactions between hydroperoxide groups and polar moieties at the bilayer interface.

The addition of the oxidized group to the unsaturated chains results in an increment in the excluded volume for these tails. The increase in the cross sectional area (Table 1) is dependent on the excluded volume and accommodation of the hydroperoxide group in the interfacial region. The similarity between the experimental Weber et al. [93]) and simulation values for the DOPC-2OOH bilayer is noteworthy, suggesting that this species could be present in high concentrations in the experimental measurements [93].

2.1.2. Monolayers

Literature is scarce regarding the use of monolayers as biomimetic interfaces to explore the properties of lipid oxidation, both experimentally [8,41,73], and computationally [36].

In the latter work, aldehyde products were simulated by cleavage of the DOPC tail at the unsaturated carbon, thus forming aldehyde derivatives like nonanal. Like the bilayer systems, the authors reported surface expansion for mixtures ranging from 10% to 100% of OxPLs, with subsequent condensation of the monolayers. The authors ascribed the phenomena to nonanal leaving the monolayer, corroborating experimental observations [82]. In the extreme case of 100% oxidized lipid, monolayers dissolved into micelles. Like in the bilayer systems, water permeated into the oxidized lipid regions in the monolayer systems.

To unveil similarities and differences between the results in monolayers *versus* lipid bilayers, here we present results of all-atom MD simulations of lipid hydroperoxidation effect on DOPC (allowing a liaison with those presented in Section 2.1.1) and Cardiolipin (CLP) monolayers. The hydroperoxide group was attached at carbon 9 and the phospholipids derivatives were those with one and two of these groups, herein referred to as DOPC-OOH, DOPC-2OOH, CLP-OOH and CLP2-OOH. Structures can be visualized in Scheme 1.

The CHARMM36 force field and TIP3P water model were used in the simulations. The same set of parameters used to describe the hydroperoxide group in the bilayers simulations was also used in the monolayer simulation, which were simulated in a slab type arrangement. Detailed information about all computational procedures, as well as a figure illustrating the slab type arrangement can be found in SI.

Like hydroperoxized *bilayers*, monolayers with oxidized derivatives of DOPC and CLP experience altered physicochemical properties. Prior simulations data of area expansion in hydroperoxized phospholipid monolayers, as well as data relating the area expansion in monolayers *versus* bilayers, are nonexistent.

The percentage area expansion due to hydroperoxidation of DOPC is greater for monolayers than for bilayers (Tables 1 and 2). The highest percentage increase was about 6.7% and 5.8%, for the first and for the second hydroperoxidation. Bilayers exhibit an attractive term between the lipid tails of opposite leaflets, not present in monolayers [52]. Therefore, monolayers tend to expand more due to internal lateral pressure (originating from repulsive interactions between the lipids) than bilayers.

The percentage area increase is similar for CLP-OOH (one out of 4 tails oxidized) and DOPC-OOH (one out of 2 tails oxidized). Similarly, the percentage area increase of CLP-2OOH (2 out of 4 tails oxidized) and DOPC-2OOH (both tails oxidized) is similar. This can be understood by taking into account two factors: (i) the tails are the same, derived from the oleic acid and (ii) DOPC's tail has a sectional area of ~33 Å^2 whereas CLP's tail has a sectional area of ~27 Å^2. Interestingly, the second hydroperoxidation provides the same area percentage increase (approximately 10%), independent of the membrane mimetic model (monolayer *versus* bilayer) and headgroup.

As pointed out in Section 2.1.1, the permeation of water seems to be a well-established consequence of the oxidation processes, and is expected when a hydrophilic group resides in the bilayer interior. Fig. 4 shows site–site radial distribution functions between carbon 9 and water. (See Fig. 5.)

For both DOPC and CLP, the first hydroperoxidation has a higher peak intensity in than that for the bi-hydroperoxides. Integrating the site-site radial distribution function around the well-defined peak, we

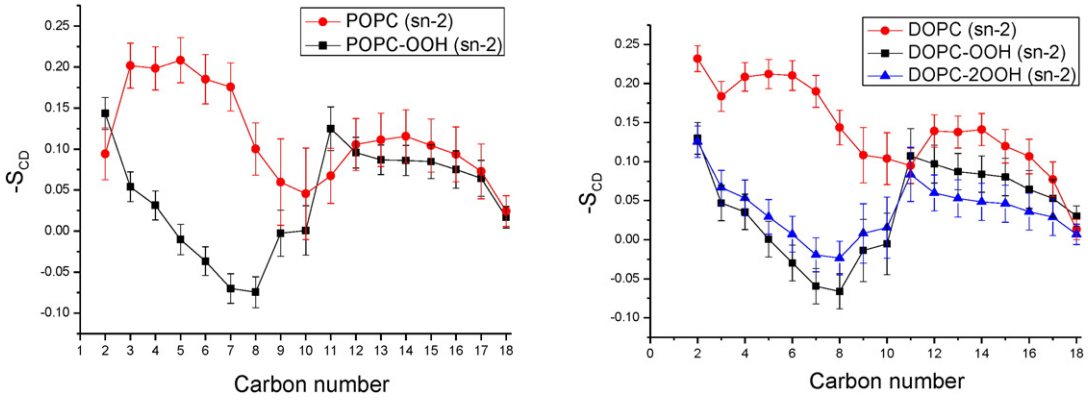

Fig. 2. Order parameter for *sn*-2 chains of DOPC, POPC and their hydroperoxized products, DOPC-OOH, DOPC-2OOH and POPC-OOH. Left: POPC and POPC-OOH. Right: DOPC, DOPC-OOH and DOPC-2OOH.

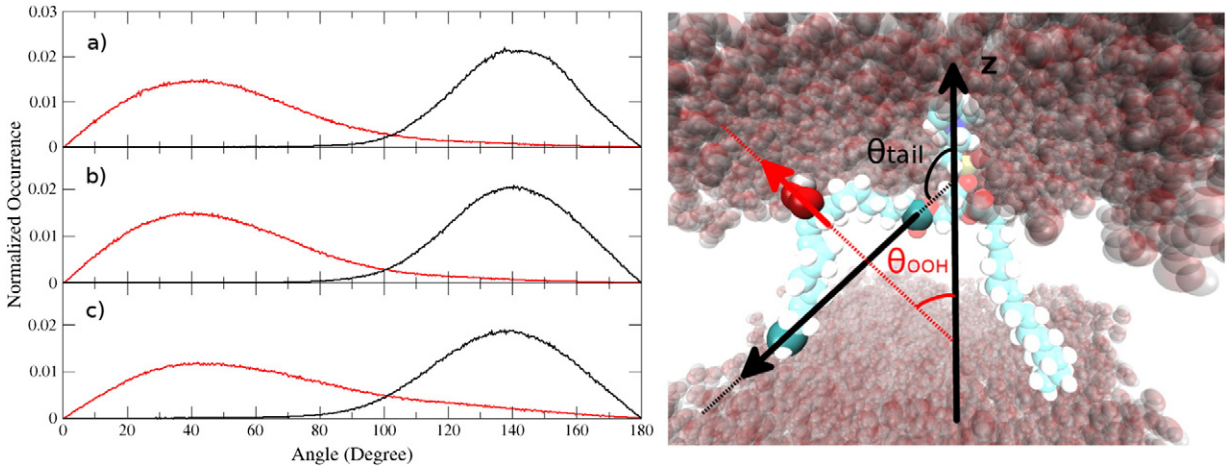

Fig. 3. Tilt angle distributions of *sn*-2 oxidized chains and hydroperoxide vector with respect to the bilayer normal. The POPC-OOH, DOPC-OOH and DOPC-2OOH results are presented in a, b and c, respectively. The red curve corresponds to Θ_{tail} angles, and the black curve to the Θ_{OOH} angles.

find that there is one water molecule on average solvating the hydroperoxide group. The electron density profiles also show that hydroperoxidation of both tails does not trigger higher water penetration in the hydroperoxide region.

2.2. Coarse-grained simulations

All-atom simulations have shed considerable light on the impact of lipid oxidation on the structural properties of pure lipid bilayers. However, lipid oxidation can also affect phase segregation in bilayers (for references, see [38]) and alter bilayer mechanical properties: phenomena that are better investigated using coarse-grained (CG) MD simulations. For lipid systems, the MARTINI force field [49–51,65] is most popular for CG simulations. Like in most coarse graining procedures, information about dynamics becomes unavailable. In the following section, we will first review the limited literature on OxPL CG-MD simulations, and then describe some of our recent results which show that the ELBA lipid force field [18,59–62] does a better job than MARTINI in reproducing properties of OxPL systems, while apparently also retrieving the dynamics of the systems correctly.

2.2.1. Simulations with MARTINI

In MARTINI, four heavy atoms plus hydrogen atoms are (on average) mapped onto one soft sphere bead (Lennard-Jones 12–6 potential). Charged groups interact by a screened term with a relative dielectric constant of 15. Polarizable water models were developed for MARTINI, to be used with a relative dielectric constant of 2.5 [97], and the big multipole water model to be used with a relative dielectric constant of 1.3 [96]. In studies involving compounds resulting from oxidative biological processes using MARTINI, it was suggested by Khandelia et al. [38]) that the protection of the mammalian membranes from lipid oxidation products, more specifically the 1-palmitoyl-2-azelaoyl-*sn*-glycero-3-phosphocholine (PazePC) lipids, is due to shape complementary with cholesterol, leading to sequestration of PazePC lipids into cholesterol-PazePC rich regions.

MARTINI was also utilized in the hydroperoxized POPC and DOPC MD simulations by Guo et al. [25]), where bilayers for these lipids were modeled and compared to the experimental data. A decrease in the stretching modulus and in the lipid lateral diffusion constant was observed after hydroperoxidation. The results also suggest that the relative increase in the area per lipid after peroxidation process is recurrent and independent of the OxPLs type.

2.2.2. Simulations with the ELBA force field

ELBA (ELectrostatic-BAsed) is a coarse-grained force field of phospholipids and water where the water model is based on a Lennard-Jones soft sphere plus a permanent point dipole and phospholipids are described by Lennard-Jones beads plus charges and point dipoles. The key feature of ELBA is its correct (and natural) treatment of electrostatic interactions through a relative dielectric constant of one. The main disadvantage (currently) is a limited time step of 10 fs.

In this context, we also compare the performance of ELBA and the popular MARTINI force field. ELBA has important features compared to other coarse grained force fields: i) it is a top-down coarse procedure motivated by a correct electrostatic treatment of interactions and shielding provided by ELBA water molecules; ii) the ELBA water model is a one-to-one mapping from typical molecular water models, preserving its dipolar nature and van der Waals volume; and iii) electrostatics of phospholipids are described by point monopoles and dipoles giving a more detailed representation of the electrical field from headgroups. Thus, ELBA provides a simple and correct interpretation for phenomena such as solvation of phospholipids, permeation of water molecules through bilayers, membrane potential as well as lateral diffusion of phospholipids.

We developed an extension of the ELBA parameters for POPC and hydroperoxized phospholipids, whose ELBA representation is shown in Fig. 6. In short, our description for the hydroperoxide group is a Lennard-Jones sphere having parameters that reflect the hydroperoxide volume and an embedded point dipole.

Table 1
Increase of the average area per phospholipid after hydroperoxidation in comparison to the non-OxPLs analogs.

	POPC-OOH	DOPC-OOH	DOPC-2OOH
Theoretical value	15.0%	11.0%	21.6%
Experimental value	15.6%	19.1%	

Table 2
Simulation and experimental average areas per phospholipid (in $Å^2$ per lipid) for DOPC, CLP and hydroperoxized derivatives (DOPC-OOH, DOPC-2OOH, CLP-OOH and CLP-2OOH) at a surface pressure of 20 $mN \cdot m^{-1}$.

System	Simulation area	Percentage increase	Experimental area[a]
DOPC	64.8 ± 1.1	–	~65
DOPC-OOH	76.2 ± 1.2	17.7	–
DOPC-2OOH	82.5 ± 1.4	27.4	–
CLP	109 ± 0.8	–	~110
CLP-OOH	125.7 ± 1.3	15.3	–
CLP-2OOH	135.9 ± 1.4	25.6	–

[a] Schmidt et al. [75]).

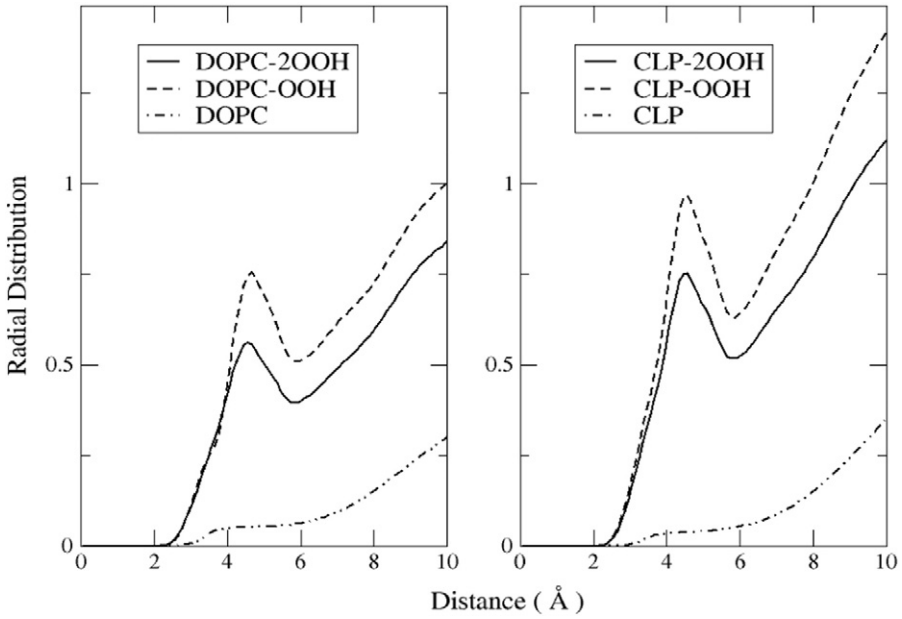

Fig. 4. Site–site radial distribution functions between water and the carbon atom attached to the hydroperoxide group.

We studied the following products of the lipid peroxidation process: POPC-OOH, DOPC-OOH and DOPC-2OOH, and their mixtures composed of POPC:POPC-OOH (1:1) and DOPC:DOPC-OOH (1:1). All ELBA simulation analyses were obtained from systems containing 128 lipids (with the exception of bilayer compressibility (K_A) also calculated for systems containing 1058 lipids). More details about the simulation protocol and parameters are available in the SI.

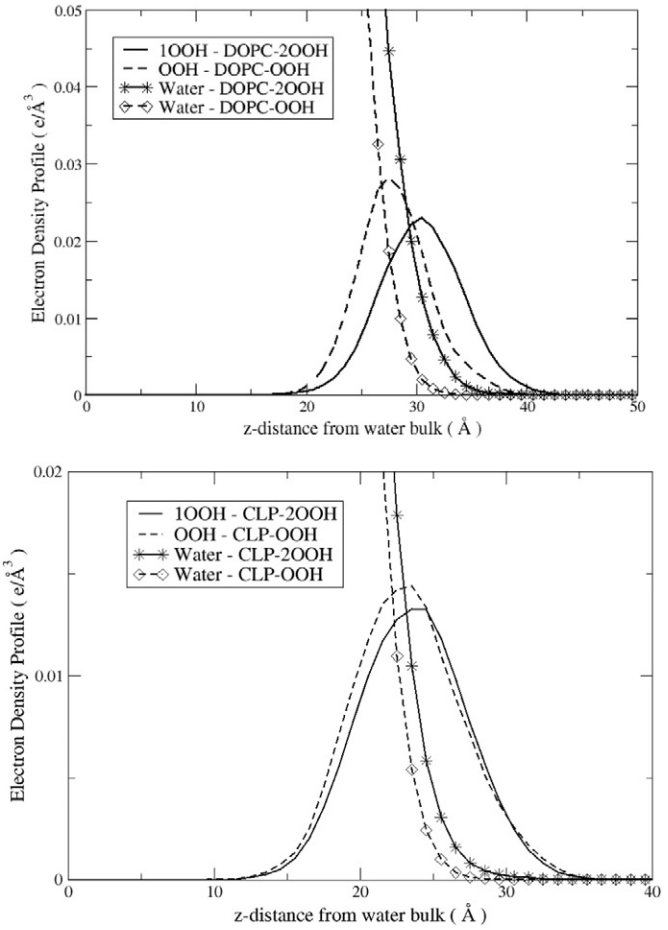

Fig. 5. Electron density profile for water and the hydroperoxide group in the DOPC-OOH, DOPC-2OOH, CLP-OOH and CLP-2OOH monolayer systems. For bi-hydroperoxide compounds the EDP curves for one (of two) hydroperoxide group were plotted.

The simulation EDP profiles (Fig. 7) are in qualitative agreement with Small-Angle X-ray diffraction measurements [53]. There is an increase in the membrane core density and the EDP maximum is displaced towards the membrane center. The hydroperoxide group profiles have a unimodal behavior for each bilayer leaflet.

The position for the maxima of the hydroperoxide group, between 7 and 10 Å with respect to the bilayer center, and the increase in water penetration below the headgroup, 5 Å near the membrane core, are in line with all-atom force field predictions (Fig. 1, Section 2.1.1).

We estimated the average number of water molecules that spontaneously permeated the bilayer. For pure POPC and DOPC lipid bilayers, the results were 11 ± 3 molecules μs^{-1} nm^{-2} and 6 ± 1 molecules μs^{-1} nm^{-2}, respectively. For pure POPC-OOH, higher water permeation was found with a ratio of 2230 ± 14 molecules μs^{-1} nm^{-2} in comparison to 365 ± 22 molecules μs^{-1} nm^{-2} for DOPC-OOH bilayer. POPC:POPC-OOH (1:1) and DOPC:DOPC-OOH (1:1) mixed bilayers showed 1121 ± 84 molecules μs^{-1} nm^{-2} and 238 ± 14 molecules μs^{-1} nm^{-2}, respectively. For DOPC-2OOH bilayer, the number was 1057 ± 64 molecules μs^{-1} nm^{-2}. Snapshots (after 1.5 μs) of water permeation through POPC and POPC-OOH bilayers are shown in Fig. 8.

The free energy cost of transporting one ELBA water molecule across the bilayer was calculated using the adaptive force biasing technique (see SI for computational details). Without oxidation, the free energy to pull a water molecule from aqueous bulk to the interior of the POPC and DOPC bilayers was 5.5 ± 0.5 kcal mol^{-1} and 6.5 ± 0.4 kcal mol^{-1}, respectively. For pure POPC-OOH or DOPC-OOH bilayers, the numbers were 3.7 ± 0.2 kcal mol^{-1} and 4.2 ± 0.1 kcal mol^{-1}, respectively (Fig. 9). The average decrease in the free energy difference obtained with the hydroperoxidation process on the POPC and DOPC bilayers were ~2 kcal mol^{-1}. A similar decrease was reported [94] for pure and non-oxidized to OxPLs (1:1) mixtures derived from PLPC lipid using all-atom simulation, from 0.96 kcal mol^{-1} to 2.65 kcal mol^{-1}.

Interestingly, the free energy of transfer of one water molecule from aqueous bulk to the membrane core is the same for the mixed POPC:POPC-OOH (1:1) and DOPC:DOPC-OOH (1:1) bilayers and the pure hydroperoxized systems. When half the lipids are oxidized, each

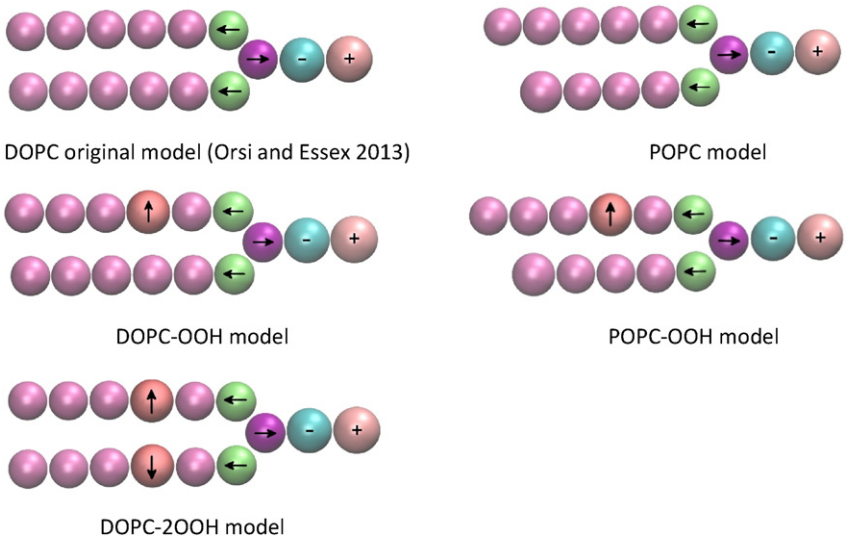

Fig. 6. ELBA representation for DOPC, DOPC-OOH, DOPC-2OOH, POPC and POPC-OOH models.

POPC or DOPC lipid is surrounded by at least one oxidized lipid. Thus, a water molecule traversing through the bilayer always has a hydroperoxide group available for hydrogen bonding, both in the 1:1 mixed systems and the pure oxidized systems.

For both mixtures and pure systems, hydroperoxide groups prefer to coordinate with other hydroperoxide groups, headgroup ester groups and water molecules, in that order. The same behavior was confirmed by atomistic simulation (see SI). In particular, interactions with water molecules are much weaker than interactions with other hydroperoxide and ester groups (Fig. 10).

Literature is divided with regard to the effect of OxPLs on lateral lipid mobility in bilayers. The theoretical and experimental results obtained by Beranova et al. [6]) comparing POPC bilayers and mixtures containing POPC and 10% of truncated *sn*-2 tail with charged carboxylic (PGPC) or aldehyde group (POVPC), showed an increase in lipid mobility. On the other hand, OxPLs with non-cleaved chains did not show significant change in the lipid diffusion coefficient measured by fluorescence correlation spectroscopy [34].

In SUVs containing DOPC mixed with 1-stearoyl-2-arachidonoyl-*sn*-glycero-3-phosphocholine (SAPC), a highly unsaturated phosphocholine containing four double bonds, the diffusion constant decreased with an increasing concentration of OxPL (Borst et al. [10])).

We calculated the lateral diffusion constants using both the MARTINI and ELBA force fields. (see SI for detailed procedures).

The lateral diffusion constants from the ELBA simulations are in very good agreement with experimental data for POPC and DOPC bilayers (Table 3). Lateral diffusion coefficients calculated from MARTINI are off by an order of magnitude (10 times higher). Interestingly, ELBA simulations also show an increase in the diffusion coefficient following hydroperoxidation, while in MARTINI the opposite effect is observed [25].

We checked for the formation of nanoaggregates in the mixture simulations using the approach of de Vries [17], which finds the probability of occurrence of a specific lipid within the first four nearest neighbor of a reference lipid (see Table 4).

For both systems, there is no evidence of nanoaggregates, indicating that the mixtures are near-ideal. The site-site radial distribution function between glycerol groups for hydroperoxized and non-hydroperoxized lipids in the 1:1 mixture are also identical, corroborating the nearest-neighbor analysis (see SI).

Complete hydroperoxidation of POPC and DOPC induces significant changes in the elastic properties of GUVs [93]. The stretching modulus (K_a) for POPC and DOPC GUVs obtained by the micropipette technique is about 200 mN m^{-1}. The value reduced to 50 mN m^{-1} after complete

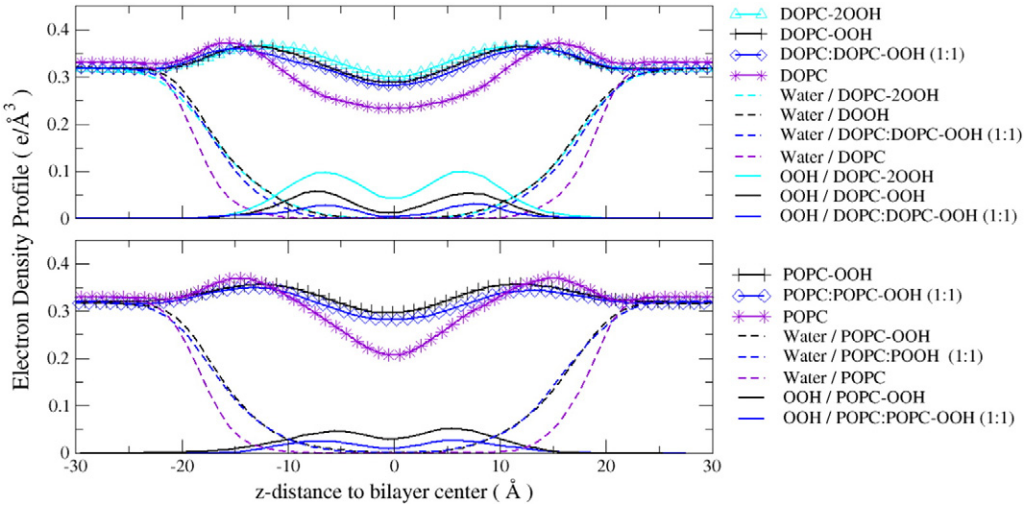

Fig. 7. Electron density profile for POPC, POPC-OOH, POPC:POPC-OOH (1:1), DOPC, DOPC-OOH, DOPC-2OOH and DOPC:DOPC-OOH (1:1) bilayers.

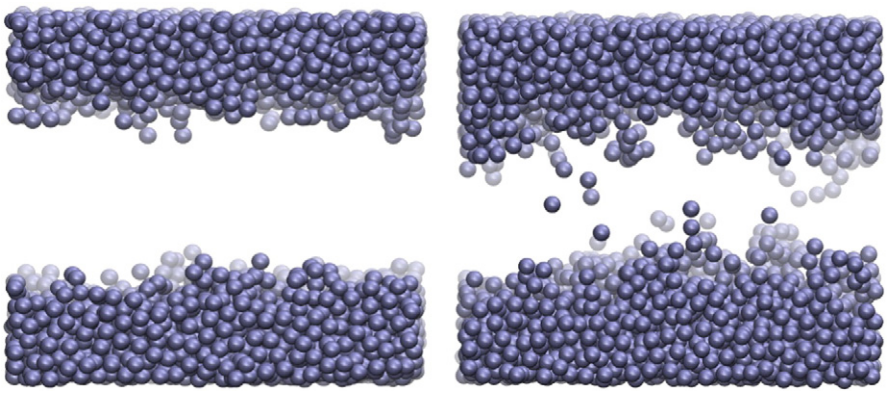

Fig. 8. Snapshot for ELBA water beads after 1.5 μs of MD simulation for POPC (left) and POPC-OOH (right) bilayers:

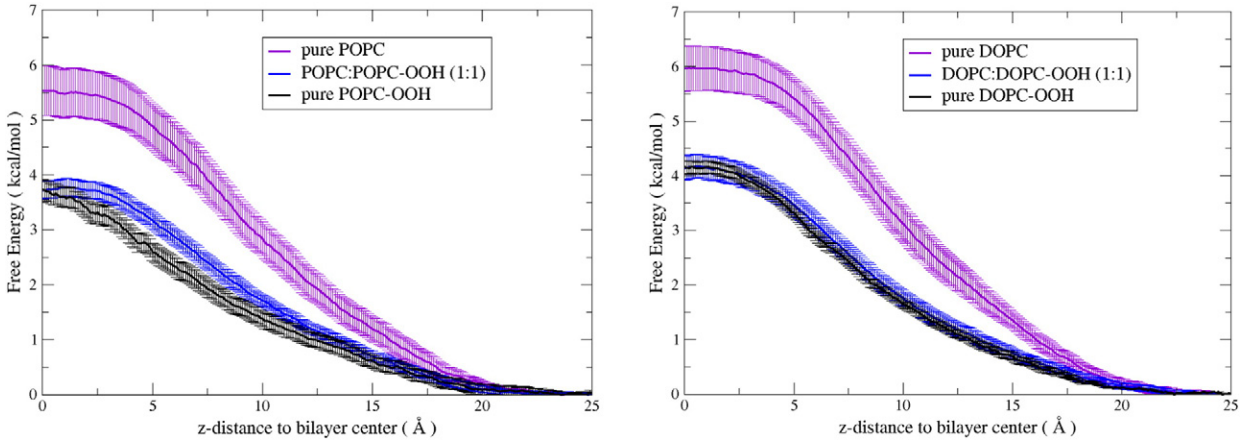

Fig. 9. Free energy profile for water permeation across ELBA bilayers. Left: POPC systems. Right: DOPC systems.

hydroperoxidation of POPC and to 150 mN m^{-1} when 35% of DOPC was hydroperoxized. The linear dependence between the hydroperoxide lipid conversion rate and the stretching modulus was confirmed by single-chain mean field theory. Both MARTINI [25] and ELBA simulations (see SI for more details) confirm a reduction in the stretching modulus (Table 5).

The elasticity of bilayers are closely related in regulation of $GABA_A$ receptor function [77] and also on lipid–peptide interactions [37]. A linear decrease in the free energy of binding of amphipathic peptides to bilayers with increasing bilayer stretching modulus was verified in the study of Vidal and McIntosh [88]). The decrease observed in the K_a for the OxPLs bilayers (Table 5) suggest a minor cohesion in the membrane plane between OxPLs molecules. The opposite pattern, an increase in the cohesive interaction in the bilayer plane was observed by Allende et al. [1]) when cholesterol was added into PC bilayers.

We have seen a discrepancy about two times greater for the stretching modulus than the experimental measurements by Rawicz [67] for both ELBA and MARTINI CG systems containing less than 512 lipids. It was demonstrated [90] that the stretching modulus calculations obtained from explicit simulations of lipid bilayers, despite

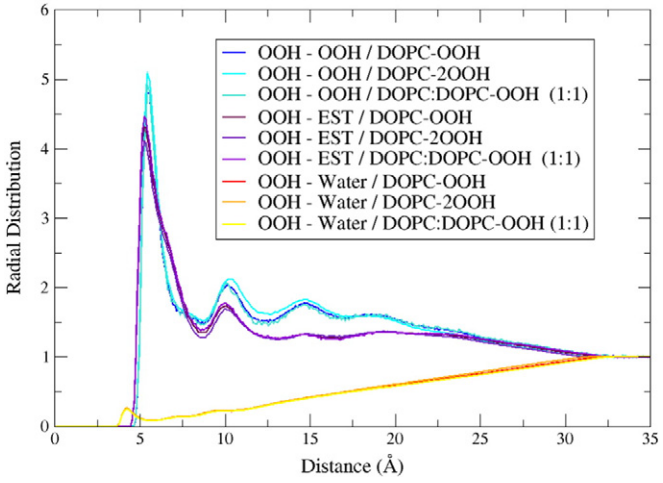

Fig. 10. Site–site radial distribution function between beads representing water molecules, hydroperoxides and ester groups.

Table 3
Lateral diffusion coefficients for pure POPC, DOPC, POPC-OOH, DOPC-OOH, DOPC-2OOH and POPC:POPC-OOH (1:1) and DOPC:DOPC-OOH (1:1) mixtures (in $\mu m^2\ s^{-1}$). ELBA simulations used 128 phospholipids. MARTINI simulations were carried out using 512 phospholipids.

System	ELBA force field	MARTINI force field[a]	Experimental data
POPC	2.57 ± 1.52	40.2 ± 2.6	7 ± 3[c]
POPC-OOH	7.29 ± 1.21	32.2 ± 2.2	–
POPC:POPC-POOH	8.65 ± 2.22	–	–
DOPC	3.19 ± 2.59	34.5 ± 1.5	4.2 ± 0.4[b]
DOPC-OOH	6.98 ± 1.45	–	–
DOPC:DOPC-OOH	9.02 ± 1.76	–	–
DOPC-2OOH	8.18 ± 1.25	24.4 ± 2.2	–

[a] [25].
[b] [5].
[c] [23].

Table 4
Fraction of a particular phospholipid "i" around a reference lipid "j" ($f_{i,j}$) using nearest-neighbor analysis for 1:1 mixtures between POPC:POPC-OOH and DOPC:DOPC-OOH bilayers. 2 μs of MD simulations using 128 ELBA lipids were used in the analysis.

System	$f_{non\text{-}OxPl,non\text{-}OxPl}$	$f_{OxPl\text{-}OxPl}$
POPC:POPC-OOH	0.500	0.500
DOPC:DOPC-OOH	0.497	0.503

including undulation corrections, are ~50% larger than experiments and hence there is a noteworthy system size-dependency.

Meanwhile, both MARTINI and ELBA showed small numbers for the stretching modulus in larger systems (the undulation correction is neglected for ELBA results), as a direct consequence of recurrent effect of fluctuations on larger bilayer systems sampled for long times, extensively discussed in the literature [3,14,45,48,49,76].

We also noted a decrease in the mean square fluctuation in the instantaneous pressure when the number of lipids (and consequently the volume) in our ELBA models were extended by one order of magnitude, confirming the observation by Landau and Lifshitz [44]) that the mean square fluctuation of additive thermodynamic quantities are inversely proportional to the square root of the total system volume. Thus, we found a minor uncertainty in the area fluctuations (standard deviation) as well as a slight decrease in the average area per lipid with increase of ELBA bilayers (Table 5).

3. Concluding remarks

Molecular level understanding of the physical changes imparted on cell membranes due to the generation of oxidized lipid species within the membranes is of paramount importance. In fact, many investigations are dealing with the roles of lipid oxidation in physiological and pathological processes. Much has been learnt by simulation and experiments about oxidized lipids and their influence on liposomes made up of lipid bilayers in the last decade. Information and properties at molecular level often inaccessible by experimental techniques could be inferred by computational simulation techniques, and experiments have validated simulations.

Here, in particular, we emphasize upon the common features obtained in simulations of hydroperoxized lipid bilayers and monolayers. There is an increase in hydration and lateral area. A well-defined and consistent position of the electron density distribution for hydroperoxide groups was obtained for both bilayers and monolayers, even after repeated oxidation. There was a noted absence of pore formation. With hydroperoxide tails, there was a specific anchoring effect, which keeps them internalized in the membrane core despite the strong attraction of the polar group towards the bilayer interface. Compared to nonoxidized tails, a reduction of the order parameters in the carbon bonds preceding the hydroperoxide group was observed, without significant changes in the tail region below the hydroperoxide group. The membrane changes are accompanied by a decrease of membrane bilayer thickness and elastic modulus. All of the above results are in good agreement with experiments.

The motivation for ELBA simulations came from its more accurate treatment of electrostatic interactions involving water molecules and membranes. Like experiments, simulations with the ELBA force field show an increased lateral diffusion constant upon hydroperoxidation, while MARTINI diffusion coefficients decrease, contrary to expectation.

The better comprehension of the physico-chemical changes in lipid model systems induced by oxidation opens a window of opportunities in the use of the knowledge in new technologies. For instance, new disease treatments that aim to protect membranes from photo-oxidative damage, and new strategies for drug delivery by controlling permeability can benefit from the simulations.

Table 5
Comparison of the stretching modulus (K_a) and between ELBA FF and MARTINI FF.

	ELBA force field with 128 lipids	ELBA force field with 1058 lipids	MARTINI force field with 512 lipids	MARTINI force field with 8192 lipids
	Ka(mN/m)	Ka(mN/m)	Ka(mN/m)	Ka(mN/m)
POPC	403 ± 8	159 ± 12	379 ± 21	245 ± 42
POPC:POPC-OOH	229 ± 12	48 ± 2	–	–
POPC-OOH	209 ± 5	44.05 ± 4	211 ± 11	104 ± 25
DOPC	488 ± 7	302 ± 9	357 ± 19	230 ± 27
DOPC:DOPC-OOH	300 ± 10	138 ± 2	–	–
DOPC-OOH	275 ± 6	42 ± 10	–	–
DOPC-2OOH	232 ± 2	89 ± 44	103 ± 12	73 ± 7

Transparency document

The Transparency document associated with this article can be found in online version.

Acknowledgements

This work is supported by grants from CNPq-Brazil and FAPESP (grant no 2012/50680-5). PS thanks CNPq-Brazil for a sandwich doctoral fellowship (process number 234433/2014-0). LGD and PS are grateful to Prof. Mario Orsi (School of Engineering & Material Science, Queen Mary University of London) for the comments and suggestions about ELBA force field. Computations were carried out at the USP High Performance Computing (USP — HPC), UFABC High Performance Computing (UFABC — HPC) and Danish e-Infrastructure Cooperation (DeIC). RI is a recipient from CNPq research fellowship. HK is funded by a Lundbeckfonden Young Investigator Grant.

Appendix A. Supplementary Information

Supplementary data associated with this article (Molecular dynamics simulation protocols, free energy approach, lateral self-diffusion analysis etc.) can be found in the online version, at http://dx.doi.org/10.1016/j.bbamem.2016.03.031.

References

[1] D. Allende, et al., Melittin-induced bilayer leakage depends on lipid material properties: evidence for toroidal pores, Biophys. J. 88 (3) (2005) 1828–1837.
[2] C. Arnarez, et al., Dry martini, a coarse-grained force field for lipid membrane simulations with implicit solvent, J. Chem. Theory Comput. 11 (1) (2014) 260–275.
[3] G. Ayton, G.A. Voth, Bridging microscopic and mesoscopic simulations of lipid bilayers, Biophys. J. 83 (6) (2002) 3357–3370.
[4] A.G. Ayuyan, F.S. Cohen, Lipid peroxides promote large rafts: effects of excitation of probes in fluorescence microscopy and electrochemical reactions during vesicle formation, Biophys. J. 91 (6) (2006) 2172–2183.
[5] A. Benda, et al., How to determine diffusion coefficients in planar phospholipid systems by confocal fluorescence correlation spectroscopy, Langmuir 19 (10) (2003) 4120–4126.
[6] L. Beranova, et al., Oxidation changes physical properties of phospholipid bilayers: fluorescence spectroscopy and molecular simulations, Langmuir 26 (9) (2010) 6140–6144.
[7] O. Berger, et al., Molecular dynamics simulations of a fluid bilayer of dipalmitoylphosphatidylcholine at full hydration, constant pressure, and constant temperature, Biophys. J. 72 (5) (1997) 2002.
[8] É. Boisselier, et al., Effect of oxidation of polyunsaturated phospholipids on the binding of proteins in monolayers, Colloids Surf. B: Biointerfaces 109 (2013) 109–114.
[9] P. Boonnoy, et al., Bilayer deformation, pores, and micellation induced by oxidized lipids, J. Phys. Chem. Lett. 6 (2015) 4884–4888.
[10] J.W. Borst, et al., Oxidation of unsaturated phospholipids in membrane bilayer mixtures is accompanied by membrane fluidity changes, Biochim. Biophys. Acta (BBA)-Mol. Cell Biol. Lipids 1487 (1) (2000) 61–73.
[11] W. Caetano, et al., Photo-induced destruction of giant vesicles in methylene blue solutions, Langmuir 23 (3) (2007) 1307–1314.
[12] A. Catalá, Lipid peroxidation of membrane phospholipids generates hydroxy-alkenals and oxidized phospholipids active in physiological and/or pathological conditions, Chem. Phys. Lipids 157 (1) (2009) 1–11.
[13] S.-W. Chiu, et al., An improved united atom force field for simulation of mixed lipid bilayers, J. Phys. Chem. B 113 (9) (2009) 2748–2763.

[14] S. Chiu, et al., Structure of sphingomyelin bilayers: a simulation study, Biophys. J. 85 (6) (2003) 3624–3635.
[15] R.M. Cordeiro, Reactive oxygen species at phospholipid bilayers: distribution, mobility and permeation, Biochim. Biophys. Acta Biomembr. 1838 (1) (2014) 438–444.
[16] D.H. de Jong, et al., Martini straight: boosting performance using a shorter cutoff and GPUs, Comput. Phys. Commun. 199 (2016) 1–7.
[17] A.H. de Vries, et al., The binary mixing behavior of phospholipids in a bilayer: a molecular dynamics study, J. Phys. Chem. B 108 (7) (2004) 2454–2463.
[18] W. Ding, et al., Stress testing the ELBA water model, Mol. Simul. 42 (4) (2016) 337–346.
[19] G. Fabre, et al., Synergism of antioxidant action of vitamins E, C and quercetin is related to formation of molecular associations in biomembranes, Chem. Commun. 51 (36) (2015) 7713–7716.
[20] G. Fabre, et al., Lipocarbazole, an efficient lipid peroxidation inhibitor anchored in the membrane, Bioorg. Med. Chem. 23 (15) (2015) 4866–4870.
[21] G.O. Fruhwirth, et al., Oxidized phospholipids: from molecular properties to disease, Biochim. Biophys. Acta (BBA) — Mol. Basis Dis. 1772 (7) (2007) 718–736.
[22] J. Garrec, et al., Lipid peroxidation in membranes: the peroxyl radical does not "float", J. Phys. Chem. Lett. 5 (10) (2014) 1653–1658.
[23] E. Gielen, et al., Measuring diffusion of lipid-like probes in artificial and natural membranes by raster image correlation spectroscopy (RICS): use of a commercial laser-scanning microscope with analog detection, Langmuir 25 (9) (2009) 5209–5218.
[24] A.W. Girotti, T. Kriska, Role of lipid hydroperoxides in photo-oxidative stress signaling, Antioxid. Redox Signal. 6 (2) (2004) 301–310.
[25] Y. Guo, et al., Peroxidised phospholipid bilayers: insight from coarse-grained molecular dynamics simulations, Soft Matter 12 (1) (2016) 263–271.
[26] C.K. Haluska, et al., Photo-activated phase separation in giant vesicles made from different lipid mixtures, Biochim. Biophys. Acta Biomembr. 1818 (3) (2012) 666–672.
[27] A. Hermetter, et al., Conformations of double-headed, triple-tailed phospholipid oxidation lipid products in model membranes, Biochim. Biophys. Acta Biomembr. 1828 (8) (2013) 1700–1706.
[28] J. Heuvingh, S. Bonneau, Asymmetric oxidation of giant vesicles triggers curvature-associated shape transition and permeabilization, Biophys. J. 97 (11) (2009) 2904–2912.
[29] J. Huang, A.D. MacKerell, CHARMM36 all-atom additive protein force field: validation based on comparison to NMR data, J. Comput. Chem. 34 (25) (2013) 2135–2145.
[30] H.I. Ingólfsson, et al., Computational 'microscopy'of cellular membranes, J. Cell Sci. 176040 (2016).
[31] R. Itri, et al., Membrane changes under oxidative stress: the impact of oxidized lipids, Biophys. Rev. 6 (1) (2014) 47–61.
[32] V. Jarerattanachat, et al., Molecular dynamics study of oxidized lipid bilayers in NaCl solution, J. Phys. Chem. B 117 (28) (2013) 8490–8501.
[33] W.L. Jorgensen, J. Tirado-Rives, Potential energy functions for atomic-level simulations of water and organic and biomolecular systems, Proc. Natl. Acad. Sci. U. S. A. 102 (19) (2005) 6665–6670.
[34] P. Jurkiewicz, et al., Biophysics of lipid bilayers containing oxidatively modified phospholipids: insights from fluorescence and EPR experiments and from MD simulations, Biochim. Biophys. Acta Biomembr. 1818 (10) (2012) 2388–2402.
[35] R. Kerdous, et al., Photo-dynamic induction of oxidative stress within cholesterol-containing membranes: shape transitions and permeabilization, Biochim. Biophys. Acta Biomembr. 1808 (12) (2011) 2965–2972.
[36] M. Khabiri, et al., Properties of oxidized phospholipid monolayers: an atomistic molecular dynamics study, Chem. Phys. Lett. 519 (2012) 93–99.
[37] H. Khandelia, et al., The impact of peptides on lipid membranes, Biochim. Biophys. Acta Biomembr. 1778 (7) (2008) 1528–1536.
[38] H. Khandelia, et al., Pairing of cholesterol with oxidized phospholipid species in lipid bilayers, Soft Matter 10 (4) (2014) 639–647.
[39] H. Khandelia, O.G. Mouritsen, Lipid gymnastics: evidence of complete acyl chain reversal in oxidized phospholipids from molecular simulations, Biophys. J. 96 (7) (2009) 2734–2743.
[40] J.B. Klauda, et al., Update of the CHARMM all-atom additive force field for lipids: validation on six lipid types, J. Phys. Chem. B 114 (23) (2010) 7830–7843.
[41] A. Korytowski, et al., Impact of lipid oxidization on vertical structures and electrostatics of phospholipid monolayers revealed by combination of specular X-ray reflectivity and grazing-incidence X-ray fluorescence, J. Phys. Chem. B 119 (30) (2015) 9787–9794.
[42] W. Kulig, et al., Cholesterol oxidation products and their biological importance, Chem. Phys. Lipids (2016) (in press).
[43] W. Kulig, et al., Cholesterol under oxidative stress—how lipid membranes sense oxidation as cholesterol is being replaced by oxysterols, Free Radic. Biol. Med. 84 (2015) 30–41.
[44] L. Landau, E. Lifshitz, Statistical Physics, Part 1: Volume 5, 1980.
[45] E. Lindahl, O. Edholm, Mesoscopic undulations and thickness fluctuations in lipid bilayers from molecular dynamics simulations, Biophys. J. 79 (1) (2000) 426–433.
[46] M. Lis, et al., The effect of lipid oxidation on the water permeability of phospholipids bilayers, Phys. Chem. Chem. Phys. 13 (39) (2011) 17555–17563.
[47] A.D. MacKerell, et al., All-atom empirical potential for molecular modeling and dynamics studies of proteins, J. Phys. Chem. B 102 (18) (1998) 3586–3616.
[48] S. Marrink, A. Mark, Effect of undulations on surface tension in simulated bilayers, J. Phys. Chem. B 105 (26) (2001) 6122–6127.
[49] S.J. Marrink, et al., Lipids on the move: simulations of membrane pores, domains, stalks and curves, Biochim. Biophys. Acta Biomembr. 1788 (1) (2009) 149–168.
[50] S.J. Marrink, et al., The MARTINI force field: coarse grained model for biomolecular simulations, J. Phys. Chem. B 111 (27) (2007) 7812–7824.
[51] S.J. Marrink, D.P. Tieleman, Perspective on the martini model, Chem. Soc. Rev. 42 (16) (2013) 6801–6822.
[52] D. Marsh, Lateral pressure in membranes, Biochim. Biophys. Acta Rev. Biomembr. 1286 (3) (1996) 183–223.
[53] R.P. Mason, et al., Effect of oxidative stress on membrane structure: small-angle X-ray diffraction analysis, Free Radic. Biol. Med. 23 (3) (1997) 419–425.
[54] J.-P. Mattila, et al., Interaction of cytochrome c with 1-palmitoyl-2-azelaoyl-sn-glycero-3-phosphocholine: evidence for acyl chain reversal, Langmuir 24 (8) (2008) 4157–4160.
[55] M. Melo, et al., Parameters for martini sterols and hopanoids based on a virtual-site description, J. Chem. Phys. 143 (24) (2015) 243152.
[56] O. Mertins, et al., Physical damage on giant vesicles membrane as a result of methylene blue photoirradiation, Biophys. J. 106 (1) (2014) 162–171.
[57] H. Mitomo, et al., Oxysterol-induced rearrangement of the liquid-ordered phase: a possible link to Alzheimer's disease? J. Am. Chem. Soc. 131 (34) (2009) 12354–12357.
[58] E. Niki, Lipid peroxidation: physiological levels and dual biological effects, Free Radic. Biol. Med. 47 (5) (2009) 469–484.
[59] M. Orsi, Comparative assessment of the ELBA coarse-grained model for water, Mol. Phys. 112 (11) (2014) 1566–1576.
[60] M. Orsi, et al., Direct mixing of atomistic solutes and coarse-grained water, J. Chem. Theory Comput. 10 (10) (2014) 4684–4693.
[61] M. Orsi, J.W. Essex, The ELBA force field for coarse-grain modeling of lipid membranes, PLoS One 6 (12) (2011), e28637.
[62] M. Orsi, J.W. Essex, Physical properties of mixed bilayers containing lamellar and nonlamellar lipids: insights from coarse-grain molecular dynamics simulations, Faraday Discuss. 161 (2013) 249–272.
[63] T. Ossman, et al., Interaction of wine anthocyanin derivatives with lipid bilayer membranes, Comput. Theor. Chem. (2015).
[64] E. Paulechka, et al., Nucleobase-functionalized graphene nanoribbons for accurate high-speed DNA sequencing, Nanoscale (2016).
[65] A.A. Polyansky, et al., Antimicrobial peptides induce growth of phosphatidylglycerol domains in a model bacterial membrane, J. Phys. Chem. Lett. 1 (20) (2010) 3108–3111.
[66] Y. Qi, et al., CHARMM-GUI martini maker for coarse-grained simulations with the martini force Field, J. Chem. Theory Comput. 11 (9) (2015) 4486–4494.
[67] W. Rawicz, et al., Effect of chain length and unsaturation on elasticity of lipid bilayers, Biophys. J. 79 (1) (2000) 328–339.
[68] T.T. Reed, Lipid peroxidation and neurodegenerative disease, Free Radic. Biol. Med. 51 (7) (2011) 1302–1319.
[69] A. Reis, et al., Separation of peroxidation products of diacyl-phosphatidylcholines by reversed-phase liquid chromatography–mass spectrometry, Biomed. Chromatogr. 19 (2) (2005) 129–137.
[70] K.A. Riske, et al., Giant vesicles under oxidative stress induced by a membrane-anchored photosensitizer, Biophys. J. 97 (5) (2009) 1362–1370.
[71] V. Ruipérez, et al., Alpha-synuclein, lipids and Parkinson's disease, Prog. Lipid Res. 49 (4) (2010) 420–428.
[72] K.A. Runas, N. Malmstadt, Low levels of lipid oxidation radically increase the passive permeability of lipid bilayers, Soft Matter 11 (3) (2015) 499–505.
[73] K. Sabatini, et al., Characterization of two oxidatively modified phospholipids in mixed monolayers with DPPC, Biophys. J. 90 (12) (2006) 4488–4499.
[74] S. Sankhagowit, et al., The dynamics of giant unilamellar vesicle oxidation probed by morphological transitions, Biochim. Biophys. Acta Biomembr. 1838 (10) (2014) 2615–2624.
[75] T.F. Schmidt, et al., Binding of methylene blue onto Langmuir monolayers representing cell membranes may explain its efficiency as photosensitizer in photodynamic therapy, Langmuir 31 (14) (2015) 4205–4212.
[76] S. Shkulipa, et al., Simulations of the dynamics of thermal undulations in lipid bilayers in the tensionless state and under stress, J. Chem. Phys. 125 (23) (2006) 234905.
[77] R. Søgaard, et al., GABAA receptor function is regulated by lipid bilayer elasticity, Biochemistry 45 (43) (2006) 13118–13129.
[78] G. Spiteller, The relation of lipid peroxidation processes with atherogenesis: a new theory on atherogenesis, Mol. Nutr. Food Res. 49 (11) (2005) 999–1013.
[79] M. Štefl, et al., Comprehensive portrait of cholesterol containing oxidized membrane, Biochim. Biophys. Acta Biomembr. 1838 (7) (2014) 1769–1776.
[80] N.A. Strobel, et al., Oxidative stress biomarkers as predictors of cardiovascular disease, Int. J. Cardiol. 147 (2) (2011) 191–201.
[81] D.-M. Telesford, et al., Reduced condensing and ordering effects by 7-ketocholesterol and 5β, 6β-epoxycholesterol on DPPC monolayers, Langmuir 31 (36) (2015) 9859–9869.
[82] K.C. Thompson, et al., Reaction of a phospholipid monolayer with gas-phase ozone at the air — water interface: measurement of surface excess and surface pressure in real time, Langmuir 26 (22) (2010) 17295–17303.
[83] D. Trachootham, et al., Targeting cancer cells by ROS-mediated mechanisms: a radical therapeutic approach? Nat. Rev. Drug Discov. 8 (7) (2009) 579–591.
[84] J.J. Uusitalo, et al., Martini coarse-grained force field: extension to DNA, J. Chem. Theory Comput. 11 (8) (2015) 3932–3945.
[85] V. Uytterhoeven, et al., Hsc70-4 deforms membranes to promote synaptic protein turnover by endosomal Microautophagy, Neuron 88 (4) (2015) 735–748.
[86] J. Van der Paal, et al., Effect of lipid peroxidation on membrane permeability of cancer and normal cells subjected to oxidative stress, Chem. Sci. 7 (1) (2016) 489–498.
[87] F.J. van Eerden, et al., Characterization of thylakoid lipid membranes from cyanobacteria and higher plants by molecular dynamics simulations, Biochim. Biophys. Acta Biomembr. 1848 (6) (2015) 1319–1330.
[88] A. Vidal, T.J. McIntosh, Transbilayer peptide sorting between raft and nonraft bilayers: comparisons of detergent extraction and confocal microscopy, Biophys. J. 89 (2) (2005) 1102–1108.

[89] R. Volinsky, et al., Oxidized phosphatidylcholines facilitate phospholipid flip-flop in liposomes, Biophys. J. 101 (6) (2011) 1376–1384.
[90] Q. Waheed, O. Edholm, Undulation contributions to the area compressibility in lipid bilayer simulations, Biophys. J. 97 (10) (2009) 2754–2760.
[91] T.A. Wassenaar, et al., Computational lipidomics with insane: a versatile tool for generating custom membranes for molecular simulations, J. Chem. Theory Comput. 11 (5) (2015) 2144–2155.
[92] T.A. Wassenaar, et al., High-throughput simulations of dimer and trimer assembly of membrane proteins. The DAFT approach, J. Chem. Theory Comput. (2015).
[93] G. Weber, et al., Lipid oxidation induces structural changes in biomimetic membranes, Soft Matter 10 (24) (2014) 4241–4247.
[94] J. Wong-Ekkabut, et al., Effect of lipid peroxidation on the properties of lipid bilayers: a molecular dynamics study, Biophys. J. 93 (12) (2007) 4225–4236.
[95] Y. Wu, et al., Flexible simple point-charge water model with improved liquid-state properties, J. Chem. Phys. 124 (2) (2006) 024503.
[96] Z. Wu, et al., A new coarse-grained model for water: the importance of electrostatic interactions, J. Phys. Chem. B 114 (32) (2010) 10524–10529.
[97] S.O. Yesylevskyy, et al., Polarizable water model for the coarse-grained MARTINI force field, PLoS Comput. Biol. 6 (6) (2010) e1000810.